



## MOTION OF DIFFUSIONLESS PARTICLES IN VERTICAL STAGNATION FLOWS—I. GENERAL MODEL AND DEPOSITION EFFICIENCY OF SPHERES

D. Broday, M. Fichman, M. Shapiro\* and C. Gutfinger

Faculty of Mechanical Engineering, Technion-Israel Institute of Technology, Haifa 32000, Israel

(Received 12 June 1995; accepted 6 March 1996)

**Abstract**—Stagnation flows have been used in many studies as fair approximations of the flow field toward a flat collector, suitable for calculation of particle deposition rates. In particular, several analytical solutions for stagnation flows are widely used to model the flow over workbenches in clean rooms, and for calculating particle deposition on semiconductor wafers. It is shown that these solutions inadequately describe the flow velocity field either far from the collector surface or in its vicinity. Trajectories of diffusionless particles, calculated on the basis of these solutions, yield particle deposition efficiency as a quantity dependent on the particle initial distance (height) from the surface.

In this study a physically realistic analytical model for the stagnation flow field over a finite flat obstacle is proposed. The flow field is approximated by a superposition of several basic solutions of potential and viscous stagnation flows. It provides an adequate description of the air velocity both far from and in the proximity of the surface. This flow field compares favorably with experimental data for air velocities collected in clean rooms over workbenches.

The proposed flow field is incorporated in a general model of motion of nonspherical particles in vertical stagnation flows over a flat finite obstacle. This model is used to simulate trajectories of diffusionless aerosol particles, to revise theoretical results on deposition efficiencies of spherical particles obtained in previous studies, and to establish their range of validity. Trajectories of spherical particles are found to possess forms, enabling definition and calculation of height-independent deposition efficiency. Calculated deposition efficiencies are compared with experimental data on particle deposition, collected in clean rooms and during sampling. Comparable calculations for elongated particles are presented in a companion paper (Part II). Copyright © 1996 Elsevier Science Ltd

### 1. INTRODUCTION

Particle transport and deposition in stagnation flows is an important problem considered in many applications including (i) deposition on wafers in clean rooms (Yuu and Jotaki, 1978; Fichman *et al.*, 1990; Peterson *et al.*, 1988; Turner *et al.*, 1989; Ramarao and Tien, 1989; Peters and Cooper, 1991), (ii) filtration in granular, fibrous and nucleopore filters (Tardos *et al.*, 1978), (iii) particle sampling, (iv) impactors (Ranz and Wong, 1952; Lesnic *et al.*, 1994), etc.

A usual way to model stagnation flows is to use known solutions of the hydrodynamic equations. These solutions (Schlichting, 1987) include the potential stagnation flow field over an infinite plate

$$u = \alpha x, \quad v = -\alpha y, \quad (1)$$

with  $\alpha$  being the shear rate coefficient, a comparable potential flow for a plate of finite width (Milne-Thompson, 1968) and a viscous stagnation flow over an infinite plate (Schlichting, 1987). Potential stagnation flows do not describe adequately the flow proximate to the surface since the velocity does not obey the no-slip condition. Moreover, in the far upstream region, the velocity field obtained for the cases of an infinite plate (viscous or potential) is nonuniform, which contradicts the experimental observations of Jinno (1986), Pui *et al.* (1990a) and Kanazawa *et al.* (1991). The above shortcomings have serious implications on the particle transport and deposition, calculated on the basis of these flow fields. Definition of the particle deposition efficiency is based upon an aerosol reference flux calculated at

\* Author to whom all correspondence should be addressed.

a far upstream location (height), say,  $y_0$ . The nonuniformity of the velocity field, pertinent to stagnation flows over an infinite flat plate, implies that either particle upstream (undisturbed) concentration or particle flux is nonuniform. As such, the calculated deposition efficiency is *height-dependent*. Particle deposition rates calculated in most previous studies (save the work of Liu and Ahn, 1987) depend on their pre-tracking location  $y_0$  (Ramarao and Tien, 1989), or on *a priori* knowledge of the far upstream concentration field (Yuu and Jotaki, 1978; Peters and Cooper, 1991). The above difficulty impacts the mere definition of the deposition efficiency as a parameter characterizing the deposition rate.

Furthermore, the shear rate,  $\alpha$ , appearing in potential and viscous stagnation flow-field approximations derived for infinite plates [see equation (1)] remains as a free parameter, which cannot be determined from the flow equations (Schlichting, 1987). On the other hand, this shear rate affects particle trajectories and their deposition efficiencies (Ramarao and Tien, 1989). This makes it difficult to interpret the calculated results. Attempts to choose this shear rate parameter in several partial situations are so far devoid of physical rationale (Peters *et al.*, 1989; Strattman *et al.*, 1988).

One of the objectives of this series of papers (see also the companion paper Broday *et al.* (1996) below referred to as Part II) is to resolve the above difficulty. Specifically, we define and calculate deposition efficiencies of diffusionless particles as height-independent quantities. Towards this goal we propose an approximation for the stagnation flow field over a flat obstacle of a finite size (i.e. a collector), which adequately describes the velocity field both in the vicinity of its surface and in the far upstream region. This flow field does not contain undetermined coefficients and enables a systematic investigation of the effects of the flow parameters and geometry, as embodied in the characteristic Reynolds number.

The proposed flow field is used to calculate the trajectories and deposition efficiencies of diffusionless spherical and elongated micron-size particles on a flat plate. Specifically, in this contribution we formulate a general model of motion and deposition of axisymmetric elongated particles in viscous flows under the influence of gravity. Deposition efficiencies are calculated for spherical particles for a wide range of sedimentation velocities. This range covers various applications including contaminant deposition in clean rooms and atmospheric sampling. The results are compared with the data calculated in previous works for viscous and potential-type stagnation flows, in order to quantify the error stemming from the use of these flow fields for calculation of the deposition rate.

In Part II trajectories and deposition efficiencies of elongated particles are calculated. The results are discussed in relation to various applications, including particle deposition in clean rooms.

## 2. AIR FLOW VELOCITY FIELD

Consider a two-dimensional undisturbed (uniform) flow with speed  $U$ , over a flat workbench of width  $2L$  (Fig. 1). The velocity field is approximated by a superposition of three two-dimensional basic flows:

$$\mathbf{u}(x, y) = \mathbf{u}_v + \mathbf{u}_p + \mathbf{u}_f, \quad (2)$$

where  $\mathbf{u}_v$  is a viscous stagnation-point flow (Schlichting, 1987),  $\mathbf{u}_p$  is a potential stagnation-point flow, and  $\mathbf{u}_f$  stands for a potential flow perpendicular to a plate of finite width  $2L$  (Milne-Thomson, 1968). All the quantities appearing above are made dimensionless using the length  $L$  and the speed  $U$  as the characteristic length and velocity, namely  $\tilde{x} = Lx$ ,  $\tilde{y} = Ly$ ,  $\tilde{\mathbf{v}} = U\mathbf{v}$ ,  $\tilde{\mathbf{u}}_i = U\mathbf{u}_i$ , wherein all dimensional quantities are marked by a tilde “ $\sim$ ”. In the coordinate system shown in Fig. 1, the velocity terms in equation (2) are expressed by

$$\mathbf{u}_v = x f' \hat{\mathbf{e}}_1 - \text{Re}^{-1/2} f \hat{\mathbf{e}}_2, \quad (3a)$$

$$\mathbf{u}_p = x \hat{\mathbf{e}}_1 - y \hat{\mathbf{e}}_2, \quad (3b)$$

$$\mathbf{u}_f = V(x, y) \left[ \cos\left(\gamma_1 - \frac{\gamma_2}{2} + \frac{\pi}{2}\right) \hat{\mathbf{e}}_1 - \sin\left(\gamma_1 - \frac{\gamma_2}{2} + \frac{\pi}{2}\right) \hat{\mathbf{e}}_2 \right], \quad (3c)$$

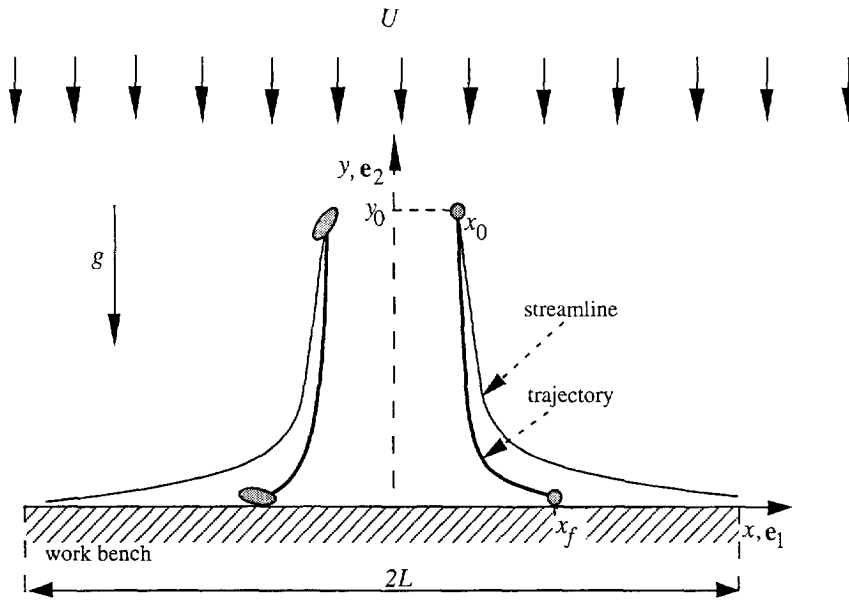


Fig. 1. Schematic of streamlines and particle trajectories in a stagnation flow over a flat surface.

where

$$V(x, y) = \frac{\sqrt{x^2 + y^2}}{4\sqrt{(x^2 - y^2 - 1)^2 + (2xy)^2}}, \quad (3d)$$

$$\gamma_1 = \tan^{-1}\left(\frac{y}{x}\right), \quad \gamma_2 = \tan^{-1}\left(\frac{2xy}{x^2 - y^2 - 1}\right), \quad (3e)$$

$Re = UL/\nu$  is the flow Reynolds number, and  $f = f(y\sqrt{Re})$  is a solution of the pertinent Falkner–Skan type problem (Schlichting, 1987). The velocity components in equation (2) are matched in the sense that

$$\mathbf{u}_v \rightarrow \mathbf{u}_p \quad \text{as } y \rightarrow \infty, \quad (4a)$$

$$\mathbf{u}_r \rightarrow \mathbf{u}_p \quad \text{as } x, y \rightarrow 0. \quad (4b)$$

Variations of the velocity with the height  $y$ , as well as the velocity due to each term on the right-hand side of equation (2), are shown, for  $x = 0$ , in Fig. 2. The flow field (2)–(4) has the following specific features: (i) The viscous part of the flow,  $\mathbf{u}_v$ , is an exact solution of the Navier–Stokes equations, and, as such, is valid for all values of Reynolds number,  $Re = UL/\nu$ . (ii) For high Reynolds number flows ( $Re \gg 1$ ) the flow has a clear boundary layer character. The dimensionless thickness of the hydrodynamic boundary layer scales as  $\delta/L = 2.4/Re^{1/2}$ . (iii) In the vicinity of the workbench mid-plane, i.e. in a region extending not too far from the stagnation line, equation (2) reproduces the exact solution  $\mathbf{u}_v$  by virtue of the corresponding matching condition (4b). In fact, the  $x$  dependence of the mismatch  $\mathbf{u}_r - \mathbf{u}_p$  at  $y = 0$  serves as a criterion for the domain of validity of equation (2). Since we are not interested in the region close to the edges ( $x = \pm 1$ ), the resulting approximation (2) appears adequate near the wall. (iv) Due to condition (4a), the velocity field (2) reproduces asymptotically  $\mathbf{u}_r$  far from the wall—a region where the flow is asymptotically uniform and its streamlines are asymptotically vertical (see Fig. 2). (v) Calculations show that the flow field (2)–(4) has a similarity property; namely, the streamlines possess the functional form

$$\frac{x}{x_0} = f(y, y_0, Re), \quad (5)$$

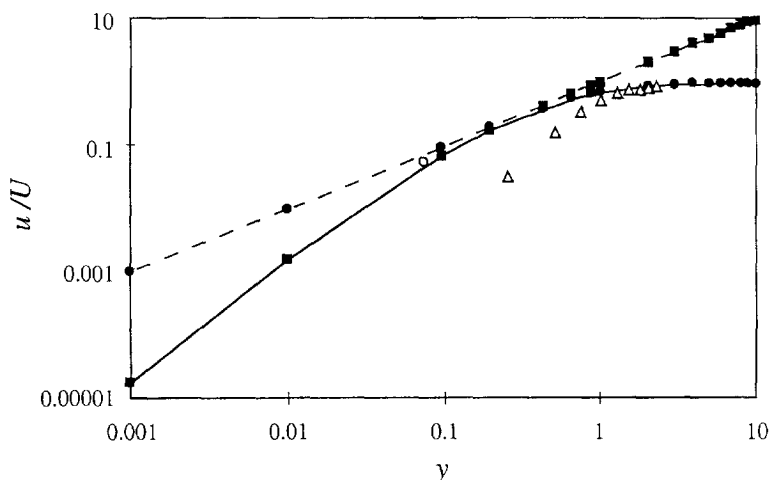


Fig. 2. Comparison between the vertical velocity components at  $x = 0$  for different stagnation flow fields,  $Re = 6700$ . Solid line—the proposed flow field (2)–(4), dashed line—potential stagnation flow, ■—viscous stagnation flow, ●—potential flow over a plate of finite width,  $\Delta$ —the experimental data of Hayakawa *et al.* (1986), ○—the experimental data of Fujii *et al.* (1988).

which, for a given Reynolds number, defines a universal streamline passing through the point  $(x_0, y_0)$ .

Matching of the flow-field components in equation (2) enables determination of the characteristic shear rate parameter  $\alpha$  [cf. equation (1)]. Indeed, expression (3b) yields  $\alpha = U/L$ , which accords with a conjecture of Strattman *et al.* (1988) on this matter. On the other hand, the choice (for clean room conditions) of Ramarao and Tien (1989) of  $\alpha = U/H$ , where  $H$  is the vertical distance between the workbench and the air flow distribution plate, is clearly incorrect.

Experimental investigations of the flow field in clean rooms had been focused mainly on streamline visualizations. Velocity measurements in clean rooms are rare and data are presented in a form which does not enable quantitative comparison with calculations. Figure 2 shows a comparison of the vertical velocity component calculated from equations (2)–(4) at the centerline of the workbench, with laboratory measurements performed over a suspended wafer inside a flow chamber (Hayakawa *et al.*, 1986; Fujii *et al.*, 1988). The flow arrangement in these experiments is three-dimensional axisymmetric and, hence, does not correspond to the present two-dimensional approximate solution (2). Nevertheless, the comparison in Fig. 2 shows that the flow field (2)–(4) represents well the measured velocity at the center of the workbench in the far region. Far from the surface, the proposed flow field is as close to the experimental data of Hayakawa *et al.* (1986) as the potential flow over a strip of finite width. It is clearly seen that both the potential and the viscous stagnation flows do not represent well the above measurements. The disagreement between the theoretical and experimental results, in the vicinity of the collector surface, may be attributed to (i) the three-dimensional flow geometry effects which are known to reduce the velocity over that in a two-dimensional configuration, (ii) experimentally uncontrolled thermally-induced secondary effects resulting from upward convective motion, and (iii) experimental errors in the measurements method as discussed by Hayakawa *et al.*

We will show below that in close vicinity of the collector surface, particle motion is dominated by gravity rather than by the local flow. Thus, particle trajectories are vertical in that region. Therefore, accurate description of the flow field very close to the deposition surface is practically unnecessary.

### 3. PARTICLE EQUATIONS OF MOTION

For dilute aerosols, particle trajectories may be calculated by neglecting (i) inter-particle hydrodynamic interactions, (ii) the Basset and added mass forces, (iii) particle-wall

hydrodynamic interactions, and (iv) short-range dispersion forces. The last two assumptions are normally used when studying the deposition of spherical particles. They are known as Smoluchowski–Levich approximations used for formulating boundary conditions for particle concentration on a wall. The validity of these assumptions for nonspherical particles is discussed in Part II.

Particle motion and deposition may be modelled by calculating their trajectories in the flowing air. For this purpose, one requires expressions for the forces and torques acting on the particles. In contrast with spheres, for nonspherical particles both translational and angular motions should be considered. Moreover, viscous hydrodynamic interactions, as well as several deposition mechanisms, e.g. those caused by interception and external forces, depend on particle shape and orientation.

Here, we formulate equations of motion for homogeneous particles, which may generally be prolate or oblate spheroids of revolution, moving in a shear flow. Let such a prolate spheroidal particle with semi-axes  $a_1 = a_3 = a$ ,  $a_2 = l > a$  and mass  $m$  be placed in a laminar vertical stagnation flow over a workbench of size  $2L$  (Fig. 1). The particle motion is modelled by the Lagrangian equations (Goldstein, 1980), with all dimensional quantities marked by a tilde “ $\sim$ ”,

$$m \frac{d\tilde{\mathbf{v}}}{d\tilde{t}} = \tilde{\mathbf{F}}_h + m\tilde{\mathbf{g}}, \quad (6)$$

$$\tilde{\mathbf{I}} \frac{d\tilde{\boldsymbol{\omega}}}{d\tilde{t}} - (\tilde{\mathbf{I}}\tilde{\boldsymbol{\omega}}) = \tilde{\mathbf{T}}_h, \quad (7)$$

where  $\tilde{\mathbf{v}}$  is the translational velocity of the particle center of mass, expressed in an inertial coordinate frame,  $\tilde{\mathbf{F}}_h$  and  $\tilde{\mathbf{T}}_h$  are viscous hydrodynamic force and torque acting on the particle,  $\tilde{\mathbf{g}}$  is the gravitational acceleration, and  $\tilde{\boldsymbol{\omega}}$  is the particle angular velocity. The torque  $\tilde{\mathbf{T}}_h$  and the inertia matrix  $\tilde{\mathbf{I}}$  appearing in equation (7) are both computed with respect to the particle center of mass, which in the present case is also the centre of hydrodynamic reaction (Happel and Brenner, 1983).

The equation of translational motion (6) is written in an inertial (laboratory) coordinate frame  $\mathbf{X}$  ( $\mathbf{e}_1, \mathbf{e}_2, \mathbf{e}_3$ ) in which the particle translational velocity  $\tilde{\mathbf{v}}$  is measured. The rotational equation of motion (7) is written in a particle-fixed (noninertial) coordinate system  $\mathbf{X}'$  ( $\mathbf{e}'_1, \mathbf{e}'_2, \mathbf{e}'_3$ ) in which the inertia matrix  $\tilde{\mathbf{I}}$  is constant. The coordinate systems  $\mathbf{X}$  and  $\mathbf{X}'$  are related by the Euler angles  $(\phi, \theta, \psi)$  via the equation

$$\mathbf{X}' = \mathbf{A}\mathbf{X}, \quad (8)$$

where  $\mathbf{A}$  is the directional cosine matrix. The particle angular velocity is related to its orientation by means of the equation

$$\tilde{\boldsymbol{\omega}} = \tilde{\boldsymbol{\omega}}(\phi, \theta, \psi). \quad (9)$$

The viscous hydrodynamic interactions of a particle in a dilute suspension are usually calculated using Stokes flow equations and assuming a quasi-static particle motion. These assumptions are valid for small particle Reynolds numbers,  $\text{Re}_p = a|\tilde{\mathbf{u}} - \tilde{\mathbf{v}}|/\nu$ , where  $|\tilde{\mathbf{u}} - \tilde{\mathbf{v}}|$  is the particle speed with respect to air of kinematic viscosity  $\nu$ , flowing with a local velocity  $\tilde{\mathbf{u}}$ . Brenner (1964) showed that the hydrodynamic force  $\tilde{\mathbf{F}}_h$  and torque  $\tilde{\mathbf{T}}_h$ , acting on an arbitrary particle in a general Stokes flow  $\tilde{\mathbf{u}}$ , can be calculated by series expansion in terms of increasing orders of the derivatives of  $\tilde{\mathbf{u}}$ . We use this series expansion (referred to below as the “generalized Faxen law”) up to terms of the order of  $(a/L)^2$ :

$$\tilde{\mathbf{F}}_h = \mu\mathbf{A}^{-1}\tilde{\mathbf{K}}\mathbf{A}[(\tilde{\mathbf{u}} - \tilde{\mathbf{v}}) + \frac{1}{6}\tilde{\mathbf{D}}^2\tilde{\mathbf{u}}], \quad (10)$$

$$\tilde{\mathbf{T}}_h = \mu[\tilde{\mathbf{Q}}(\tilde{\mathbf{R}} \times \tilde{\mathbf{u}}) - \tilde{\boldsymbol{\Omega}}_0\tilde{\boldsymbol{\omega}}]. \quad (11)$$

In the above equation  $\mu$  is the dynamic air viscosity, and  $\tilde{\mathbf{K}}$ ,  $\tilde{\boldsymbol{\Omega}}_0$  and  $\tilde{\mathbf{Q}}$  are particle hydrodynamic translational and two rotational resistance tensors, respectively. Expressions for these tensors are listed in Appendix A.

The operators  $\tilde{\mathbf{D}}^2$  and  $\tilde{\mathbf{R}}$ , appearing in equation (10) and (11), are generalized Laplacian and rotor operators written in the particle-fixed coordinate system. For ellipsoidal particles these operators are (Brenner, 1964)

$$\tilde{\mathbf{D}}^2 = a_i^2 \frac{\partial^2}{\partial \tilde{x}_i'^2}, \quad \tilde{\mathbf{R}} = a_i^2 \frac{\partial}{\partial \tilde{x}_i'} \mathbf{e}'_i, \quad (12a, b)$$

where  $a_i, i = 1, 2, 3$  are principal particle radii. Application of these operators to the velocity field in equations (2)–(4) yields

$$\tilde{\mathbf{D}}^2 \tilde{\mathbf{u}} = E_{ij} \frac{\partial}{\partial \tilde{x}_i'} \frac{\partial}{\partial \tilde{x}_j'} \tilde{u}_k \mathbf{e}_k = E_{ij} A_{im} A_{jn} \frac{\partial}{\partial \tilde{x}_m} \left( \frac{\partial \tilde{u}_k}{\partial \tilde{x}_n} \right) \mathbf{e}_k, \quad (13a)$$

$$\tilde{\mathbf{R}} \times \tilde{\mathbf{u}} = \left( E_{ij} \frac{\partial}{\partial \tilde{x}_i'} \mathbf{e}'_j \right) \times \tilde{u}_k \mathbf{e}_k = E_{ij} A_{im} A_{nk} \varepsilon_{jnl} \frac{\partial \tilde{u}_k}{\partial \tilde{x}_m} \mathbf{e}'_l, \quad (13b)$$

where  $E_{ij} \equiv a_i a_j \delta_{ij}$ ,  $\delta_{ij}$  is the Kronecker delta,  $\tilde{u}_i$  is the  $i$ th component of  $\tilde{\mathbf{u}}$ ,  $\varepsilon_{ijk}$  is the permutation tensor, and  $\mathbf{e}_i, \mathbf{e}'_i$  ( $i = 1, 2, 3$ ) are unit vectors of the coordinate systems  $\mathbf{X}$  and  $\mathbf{X}'$ , respectively. Expressions (13a, b) are written in inertial and particle-fixed coordinate systems, respectively, in accordance with the corresponding resistance terms in equation (10) and (11) required in equation (6) and (7).

In the particular case of a spherical particle, one needs only the translational equation of motion (6) to calculate the particle trajectories. This equation may be rewritten in a dimensionless form, with time normalized by  $L/U$ , spatial location  $\mathbf{x}$  of the particle center of mass ( $\mathbf{x} = x\mathbf{e}_1 + y\mathbf{e}_2$ ) normalized by  $L$  and velocities normalized by  $U$ , to obtain

$$\text{St} \frac{d^2 \mathbf{x}}{dt^2} = (\mathbf{u} - \mathbf{v}) + \frac{\sigma^2}{6} \nabla^2 \mathbf{u} - \text{Ng} \hat{\mathbf{e}}_2. \quad (14)$$

In the above,  $\sigma = a/L$  is the ratio of particle to flow characteristic lengths,  $\text{Ng} = mg/6\pi\mu aU$  is gravitational parameter, and  $\text{St} = mU/6\pi\mu aL$  is the Stokes number.

#### 4. DEPOSITION EFFICIENCY OF SPHERICAL PARTICLES

In the absence of particle rebound, the deposition efficiency on a region between the coordinates  $x_{w1}$  and  $x_{w2}$  (e.g. a wafer) is defined as

$$\eta = \frac{\int_{x_{w1}}^{x_{w2}} j_y(x, y)|_{y=\sigma} dx}{(x_{w2} - x_{w1}) j_{y\infty}}, \quad (15)$$

where  $j_y$  is the vertical component of the particle deposition flux towards the region, and  $j_{y\infty}$  is the vertical particle flux in the undisturbed region ( $y = y_0$ ), taken to be independent of  $x$ .

For diffusionless spherical particles, the integral in equation (15) may be replaced by a comparable integral at a far upstream location in terms of particle limiting trajectories. The latter begin at points  $(x_{0i}, y_0)$ , terminate at points  $(x_{wi}, \sigma)$ ,  $i = 1, 2$ , and clearly do not intersect. Therefore, all particles passing the plane  $y = y_0$  in the interval  $x_{01} < x < x_{02}$  deposit on the collector. In view of the above, one gets the following simple expression for the deposition efficiency:

$$\eta = \frac{x_{02} - x_{01}}{x_{w2} - x_{w1}}. \quad (16)$$

An alternative expression for the deposition efficiency can be obtained in terms of the deposition velocity, defined as

$$v_d = \frac{j_y|_{y=\sigma}}{N}, \quad (17)$$

where  $N$  is the concentration in the undisturbed flow. In cases where  $j_y$  in equation (15) is independent of  $x$ , as in viscous or potential stagnation flows (Yuu and Jotaki, 1978; Ramarao and Tien, 1989), the deposition efficiency  $\eta$  becomes

$$\eta = \frac{v_d}{v_y|_{y=y_0}} = \frac{v_d}{U + mg/6\pi\mu a}. \quad (18)$$

The right-hand side of equation (18) may be simplified for small particles by neglecting in the denominator the settling (sedimentation) velocity which is much smaller than the undisturbed air velocity (Liu and Ahn, 1987). In this case  $\eta = v_d/U = Ng$ , and the deposition is due to gravity only. The range of validity of this approximation is discussed in the next section.

It has been shown both for the potential stagnation flow (Yuu and Jotaki, 1978) and for the viscous stagnation flow (Ramarao and Tien, 1989) that trajectories of spherical particles are characterized by similarity property in the sense that they may be described by the equation

$$\frac{y(x, x_0, y_0)}{y_0} = \xi\left(\frac{x}{x_0}\right) = \xi(\zeta), \quad (19)$$

where  $\xi(\zeta)$  is a normalized universal trajectory. Using equation (19) one can rewrite the deposition efficiency (16) in the form

$$\eta = \frac{x_0}{x_w}, \quad (20)$$

which is independent of the collector size. This means that for given particle physical parameters and an initial height  $y_0$ , only one particle trajectory in the potential or viscous stagnation flow fields should be calculated for determination of the deposition efficiency. However, particle deposition efficiencies determined for these flows with the help of equation (19) are  $y_0$ -dependent. Therefore equation (19) cannot be used for stagnation flows, which are uniform far from the surface. As such, no universal trajectory of the form (19) exists for particles moving in the flow field (2)–(4).

Since equation (14) with the velocity field (2)–(4) cannot be solved analytically, numerical simulations of particle motion are done in order to find the pairs  $x_{0i}$  for given  $x_{wi}$  ( $i = 1, 2$ ). The objectives of the simulations, except from calculating deposition efficiencies for spherical particles, are: (i) Verify whether a universal trajectory exists for the vertical stagnation flow (2)–(4). (ii) Investigate the circumstances, in which one can calculate the deposition efficiency  $\eta$  via equation (16) as a *height-independent* quantity. (iii) Revise the previous results obtained for the deposition efficiency and establish their range of validity. The results of the simulations are described in the following section.

## 5. RESULTS AND DISCUSSION

The translational equation of spherical particle motion (14) was integrated numerically with the following initial condition

$$t = 0: \quad x = x_0, \quad y = y_0, \quad \dot{x} = 0, \quad \dot{y} = v_y|_{y=y_0}. \quad (21)$$

Simulations were terminated when the sphere touched the deposition surface, namely where  $y = \sigma$ . The comparable criterion for termination of the simulation for nonspherical particles is more complicated and is discussed in Part II. The computations were performed on a Silicon Graphics workstation using the ACSL ver. 10 ODE solver. Three different algorithms for numerical integration were checked, namely Gear's stiff variable step and variable order, Adam-Multon's variable step and variable order, and Runge-Kutta-Frehdberg's variable step and fifth order. All the algorithms yielded close results which coincided to within four significant digits.

*Particle universal trajectory:* Simulations of particle trajectories were performed for various particle initial locations  $(x_0, y_0)$ . Particle trajectories calculated for different  $x_0$  ( $x_0 < 0.05$ ) were compared, and a universal trajectory was found in the form

$$\zeta = \frac{x}{x_0} = f(y, y_0, St, Ng, Re). \quad (22)$$

This functional form of the universal trajectory is characteristic of the flow field (2)–(4), which has straight vertical trajectories far above the surface. It does not hold for the classical stagnation flows near infinite plates.

For given nondimensional parameters  $St, Ng, Re$ , all trajectories described by equation (22) coincide in the  $\zeta$ - $y$  plane (except, maybe, a vertical trajectory segment in the undisturbed far region). Trajectories which start from different  $y_0$  coincide (in the disturbed flow region) with a relative accuracy of no less than  $10^{-4}$ . As such, the dependence of  $\zeta$  upon  $y_0$  in equation (22) is unimportant. Note that the universal trajectory is found only for those particles which deposit on the collector. The range of  $x_0$  for which the universal trajectory (22) exists depends directly on the particle  $Ng$  parameter. That is, for heavier particles equation (22) holds for a wider range of  $x_0$  than for lighter particles. For example, in order that equation (22) would hold for a  $10 \mu\text{m}$  aerosol particle placed in a flow of  $U = 0.3 \text{ m s}^{-1}$ ,  $x_0$  should be smaller than about 0.05; for a  $1 \mu\text{m}$  aerosol particle placed in the same flow,  $x_0$  should be less than about  $5 \times 10^{-4}$ . This is, for small (but still diffusionless) aerosol particles the  $x_0$ -domain of validity of equation (22) is directly proportional to the square of the particle radius (see also the following paragraphs). One can directly verify that the universal trajectory in the form (22) allows to use equation (20) in calculating particle deposition efficiencies instead of equation (16).

Ramarao and Tien (1989) calculated trajectories of diffusionless particles in viscous and potential stagnation flows. They found that the effect of gravitation is to increase the deposition flux on a surface facing upward. Their results are valid for particles with  $St < 0.01$ , where the effect of inertia is negligible. That is, particle trajectories are governed only by  $Ng$ . The motion of very large particles, characterized by  $St > 1$ , is governed by  $St$  as a sole parameter, whereas the effect of gravity is negligible. This conclusion has also been drawn by Tardos *et al.* (1978) for filtration of micrometer particles by porous filters and by Ranz and Wong (1952) for aerosol motion in impactors.

Figure 3 shows trajectories of particles with small inertia ( $St < 0.01$ ). In the absence of gravity, particles move along the flow streamlines. The effect of gravity is seen to affect the trajectory only in the vicinity of the collector surface, where it forces the particles to deviate almost vertically downward. Heavier particles (characterized by larger  $Ng$ ) begin their terminal downward motion closer to the centerline. This behavior is characteristic of all viscous flows adjacent to a solid surface.

In conditions typical for clean room flows, i.e.,  $Re \sim 10^4$ , the length of the final vertical segment of particle trajectories exceeds the interception distance  $\sigma$  by a factor of about 1000. This implies that gravitation serves as the sole particle trapping mechanism and that the geometric interception is unimportant. This is true when the particle size is much smaller than the collector size, as is typical during contaminant deposition in clean rooms, atmospheric sampling, and separation by impactors (Ranz and Wong, 1952). For flows characterized by high velocities and small collector size (e.g., in gas compact heat exchangers), the above estimates may not be valid. Such flows may be approximated by pure potential flows, wherein interception may affect the deposition (Yuu and Jotaki, 1978). This also happens in the collection of coarse particles by fibrous filters (Matterson and Orr, 1987).

Our calculated results allow systematic analysis of the effect of the collector size  $L$  and flow speed  $U$  on particle trajectories and deposition mechanisms via altering the value of  $Re$ . With all other parameters fixed, increasing the flow Reynolds number helps particles to approach the collector due to increased air inertia, albeit in a manner which does not affect their final deposition sites. The latter appear to be almost independent of  $Re$  and hence of

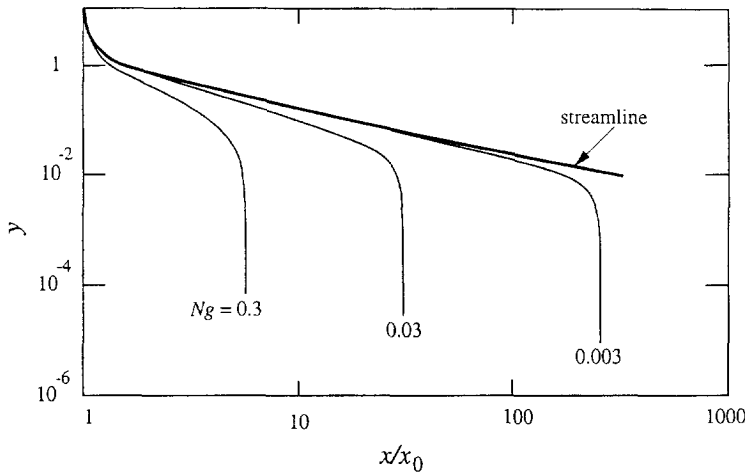


Fig. 3. Effect of the sedimentation velocity on trajectories of spherical particles,  $x_0 = 0.001$ ,  $y_0 = 10$ ,  $Re = 6700$ .

the flow field at least in the range  $10^3 < Re < 10^4$ , which accords with the conjecture of Liu and Ahn (1987) on this matter. One way to rationalize this result is to note that particle deposition efficiencies are unaffected by changing air viscosity (e.g., which may be caused by temperature changes).

*Deposition efficiencies:* Figure 4 shows a comparison of the deposition efficiency calculated via equation (20) and (22), with the results of Liu and Ahn (1987) and Ramarao and Tien (1989). Liu and Ahn (1987) calculated particle deposition velocities under the sole influence of the gravitational force. In this case equation (18) yields the relation

$$\eta = Ng, \quad (23)$$

which is shown as a dashed line in Fig. 4. One can see that this expression agrees with the present calculations for  $Ng \leq 0.2$ . In that range of  $Ng$ , equation (23) is shown to agree with the experimental data of Pui *et al.* (1990b) collected in a flow chamber and used to study deposition of micron particles in clean rooms. However, for large values of  $Ng$ , neglecting the settling velocity in the denominator of equation (18) leads to a significant overestimation of the deposition efficiency. Explicitly, one can show that  $\eta \rightarrow 1$  as  $Ng \gg 1$ , which was obtained by Ramarao and Tien (1989) who used equation (16) for the deposition efficiency. However, their deposition efficiencies depend on the particle initial height  $y_0$  since they used viscous stagnation flow over infinite plate, which is not uniform far upstream. For  $Ng > 5$  the difference between the present results and those of Ramarao and Tien (1989) amounts to 15–20%. Therefore the correct choice of the flow field in calculating deposition efficiencies is most important for large particles (i.e.,  $Ng > 1$ ).

In clean rooms, particles may be generated in the course of activities performed within the room itself. Sometimes large particles, characterized by  $Ng > 1$ , may be found. Such particles are much larger than those which normally penetrate through the HEPA filters. As a matter of fact, Gill and Dillenbeck (1989a, b) found defects in integrated circuits, caused by the deposition of contaminants of sizes of about  $40 \mu\text{m}$ . A sphere of this size has a typical  $Ng$  value of about 0.6, a value for which the deposition efficiency calculated in the present study already differs from that calculated by Ramarao and Tien (1989) by 7% and from that calculated by Liu and Ahn (1987) by 60%.

Large values of the sedimentation velocity  $Ng$  may be found in other applications such as sampling from (almost) still air by means of gravitational settling, i.e., sampling aerosols in the ambient atmosphere. The experimental data of Ralph and Barrett (1984), related to ambient atmosphere sampling, are plotted in Fig. 4. A good agreement with our theoretical curve is achieved both for low and intermediate values of  $Ng$ .

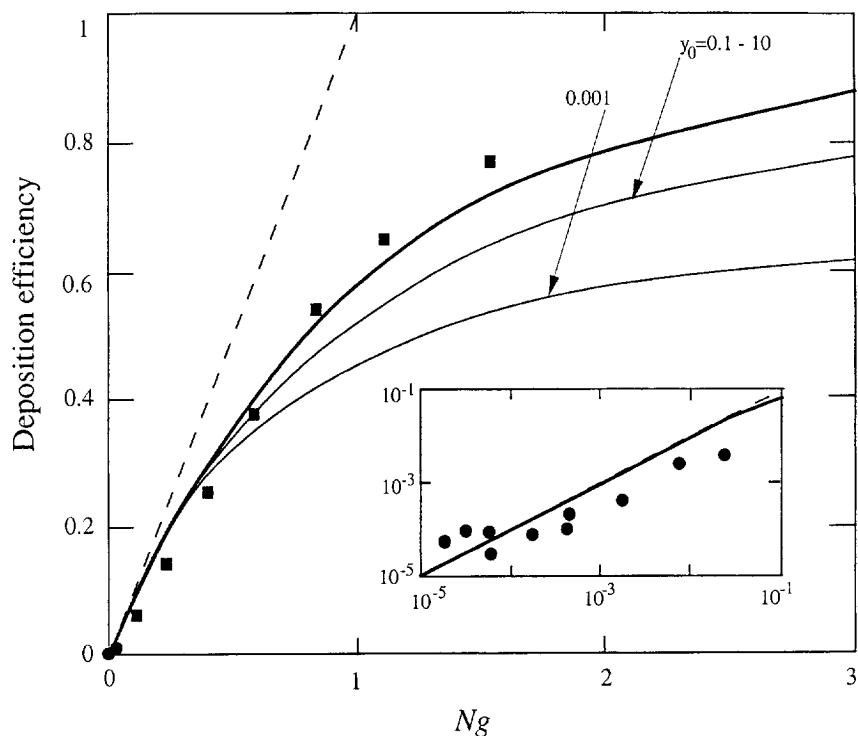


Fig. 4. Deposition efficiency of spherical particles vs dimensionless settling velocity  $Ng$ . Thick line—present results, thin lines—calculations of Ramarao and Tien (1989), dashed line—calculations of Liu and Ahn (1987). The experimental data of Ralph and Barrett (1984), relevant to atmospheric sampling, are plotted as filled squares. The region corresponding to small  $Ng$  is zoomed to show a comparison with the experimental data of Pui *et al.* (1990b), marked by filled circles, which are relevant to particle deposition in clean rooms.

## 6. CONCLUSIONS

A physically realistic velocity field (2)–(4) is proposed for modelling aerosol deposition in vertical stagnation flows. This velocity field reproduces (i) the far (undisturbed) uniform velocity far from the collector plate, and (ii) a boundary layer type flow near the collector surface. This flow field allows determination of a universal particle trajectory in the form (22) for spherical particles. Calculations of deposition efficiency  $\eta$  for spherical particles show that it is independent of both particle initial height over the collector and its initial axial location. In application to contaminant deposition in clean rooms, this means that  $\eta$  depends neither on the wafer size nor on its location on the workbench.

Deposition efficiencies calculated for inertialess particles ( $St < 0.01$ ) agree with the previous results of Liu and Ann (1987) and Ramarao and Tien (1989) for  $Ng < 0.2$ . For  $Ng \rightarrow \infty$ , which represents gravitational settling of large particles in slow air flow, the deposition efficiency tends to unity. This is in contrast with the results of Liu and Ahn (1987), which yield that  $\eta$  indefinitely grows with  $Ng$ . The geometric interception is shown to be ineffective as a capture mechanism for  $\sigma \ll 1$ . The flow Reynolds number does not influence significantly the deposition efficiency for  $Re < 7000$ , which is the range typical for clean room conditions.

The present calculation of the deposition efficiency is shown to describe satisfactorily the experimental data for spherical particle capture controlled by gravitational settling.

## REFERENCES

- Brenner, H. (1963) The Stokes resistance of an arbitrary particle. *Chem. Engng Sci.* **18**, 1–25.  
 Brenner, H. (1964) The Stokes resistance of an arbitrary particle—IV: arbitrary fields of flow. *Chem. Engng Sci.* **19**, 703–727.

- Brodoy, D., Fichman, M., Shapiro, M. and Gutfinger, C. (1996) Motion of diffusionless particles in vertical stagnation flows. Part II: Deposition efficiency of elongated particles. *J. Aerosol Sci.* **28**, 35–52.
- Fichman, M., Pnueli, D. and Gutfinger, C. (1990) Aerosol deposition in the vicinity of a stagnation point. *Aerosol Sci. Technol.* **13**, 281–296.
- Fujii, S., Xie, G., Kim, K. Y. and Hayakawa, I. (1988) Particulate reaching and deposition onto wafers. *Proc. 6th Symp. on Aerosol Science and Technology*, Japan Association of Aerosol Science, pp. 32–35.
- Gill, P. and Dillenbeck, K. (1989a) Using snake patterns to monitor defects and enhance VLSI device yields. *Microcontamination*, February, p. 23.
- Gill, P. and Dillenbeck, K. (1989b) Using snake patterns to monitor defects and enhance VLSI device yields. *Microcontamination*, March, p. 33.
- Goldstein, H. (1980) *Classical Mechanics*, 2nd Edition. Addison-Wesley.
- Happel, J. and Brenner, H. (1983) *Low Reynolds Number Hydrodynamics*. Martinus Nijhoff, The Hague.
- Hayakawa, I., Fujii, S. and Kim, K. Y. (1986) Studies on particulate behavior and adhesion in laminar airflow clean room. *IES Proc. 32nd Ann. Technical Meeting*, pp. 483–486.
- Jinno, N. (1986) Study of airflow pattern in the clean room for manufacturing semiconductors. *IES Proc. 32nd Ann. Technical Meeting*, pp. 556–564.
- Kanazawa, S., Ohkubo, T., Adachi, T., Inokuchi, M. and Shibuya, A. (1991) Flow visualization of a particle deposition on silicon wafers in clean rooms. *IEEE*, pp. 640–645.
- Lesnic, D., Elliot, L. and Ingham, D. B. (1994) The influence of separation on the collection efficiencies of obstacles. *J. Aerosol Sci.* **25**, 527–533.
- Liu, B. Y. H. and Ahn, K. H. (1987) Particle deposition on semiconductor wafers. *Aerosol Sci. Technol.* **6**, 215–224.
- Matteson, M. J. and Orr, C. (1987) *Filtration, Principles and Practices*, 2nd Edition. Marcel Dekker, New York.
- Milne-Thomson, L. M. (1968) *Theoretical Hydrodynamics*, 5th Edition. MacMillan, London.
- Peters, M. H. and Cooper, D. W. (1991) Approximate analytical solutions for particle deposition in viscous stagnation point flow in the inertial-diffusion regime with external forces. *J. Colloid Interface Sci.* **142**, 140–148.
- Peters, M. H., Cooper, D. W. and Miller, E. (1989) The effect of electrostatic and inertial forces on the diffusive deposition of small particles onto large disks: viscous axisymmetric stagnation-point flow approximations. *J. Aerosol Sci.* **20**, 123–133.
- Peterson, T. W., Sannes, K. M., Stratman, F. and Fissan, H. (1988) Particle deposition on wafers, a comparison between two modeling approaches. *J. Aerosol Sci.* **20**, 683–693.
- Pui, D. Y. H., Graztek, J. and Kuehn, T. (1990a) Experimental measurements of clean room airflow and particle transport. *IES Proc. 37th Ann. Technical Meeting*.
- Pui, D. Y. H., Ye, Y. and Liu, B. Y. H. (1990b) Experimental study of particle deposition on semiconductor wafers. *Aerosol Sci. Technol.* **12**, 795–804.
- Ralph, M. O. and Barrett, C. F. (1984) A wind tunnel study of the efficiency of three deposit gauges. Report No. LR 499 (AP), Warren Spring Laboratory, Stevenage, Herts [(1989) In *Aerosol Sampling Science and Practice* (Edited by Vincent, J. H.), Wiley, Chichester].
- Ramarao, B. V. and Tien, C. (1989) Aerosol deposition in two-dimensional laminar stagnation flow. *J. Aerosol Sci.* **20**, 775–785.
- Ranz, W. E. and Wong, J. B. (1952) Impaction of dust and smoke particles on surface and body collectors. *Ind. Engng Chem.* **44**, 1371–1381.
- Schlichting, H. (1987) *Boundary Layer Theory*, 7th Edition. McGraw-Hill, New York.
- Stratman, F., Fissan, H., Papperger, A. and Friedlander, S. K. (1988) Suppression of particle deposition to surfaces by thermophoretic force. *Aerosol Sci. Technol.* **9**, 115–121.
- Tardos, G. I., Abuaf, N. and Gutfinger, C. (1978) Dust deposition in granular bed filters: theories and experiments. *J. Air Pollut. Control Ass.* **28**, 354–363.
- Turner, R., Liguras, D. K. and Fissan, H. (1989) Clean room applications of particle deposition from stagnation flows: electrostatic effects. *J. Aerosol Sci.* **20**, 403–417.
- Yuu, S. and Jotaki, T. (1978) The calculation of particle deposition efficiency in a plane stagnation flow. *Chem. Engng Sci.* **33**, 971–978.

## APPENDIX A: HYDRODYNAMIC RESISTANCE COEFFICIENTS OF SPHEROIDS

The quantities  $\mathbf{K}$ ,  $\mathbf{\Omega}_0$ , and  $\mathbf{Q}$ , here in a dimensional form, are the particle hydrodynamic translational and two rotational resistance tensors (Brenner, 1963, 1964), given in the particle-fixed frame by

$$\mathbf{K} = 16\pi \left[ \frac{\mathbf{e}'_1 \mathbf{e}'_1}{\chi + a_1^2 \alpha_1} + \frac{\mathbf{e}'_2 \mathbf{e}'_2}{\chi + a_2^2 \alpha_2} + \frac{\mathbf{e}'_3 \mathbf{e}'_3}{\chi + a_3^2 \alpha_3} \right], \quad (\text{A1})$$

$$\mathbf{\Omega}_0 = 16\pi \left[ \mathbf{e}'_1 \mathbf{e}'_1 \frac{a_2^2 + a_3^2}{a_2^2 \alpha_2 + a_3^2 \alpha_3} + \mathbf{e}'_2 \mathbf{e}'_2 \frac{a_3^2 + a_1^2}{a_3^2 \alpha_3 + a_1^2 \alpha_1} + \mathbf{e}'_3 \mathbf{e}'_3 \frac{a_1^2 + a_2^2}{a_1^2 \alpha_1 + a_2^2 \alpha_2} \right], \quad (\text{A2})$$

$$\mathbf{Q} = \frac{16\pi}{3} \left[ \frac{\mathbf{e}'_1 \mathbf{e}'_1}{a_2^2 \alpha_2 + a_3^2 \alpha_3} + \frac{\mathbf{e}'_2 \mathbf{e}'_2}{a_3^2 \alpha_3 + a_1^2 \alpha_1} + \frac{\mathbf{e}'_3 \mathbf{e}'_3}{a_1^2 \alpha_1 + a_2^2 \alpha_2} \right], \quad (\text{A3})$$

where  $\chi$  and  $\alpha_i$  are

$$\chi = \int_0^x \frac{d\lambda}{\Delta(\lambda)}, \quad \alpha_i = \int_0^\infty \frac{d\lambda}{(a_i^2 + \lambda)\Delta(\lambda)}, \quad i = 1, 2, 3, \quad (\text{A4.5})$$

and  $\Delta(\lambda)$  is

$$\Delta(\lambda) = \sqrt{(a_1^2 + \lambda)(a_2^2 + \lambda)(a_3^2 + \lambda)}. \quad (\text{A6})$$

Note that for either orthotropic particles or bodies of revolution, these three tensors have zero off-diagonal components. For a prolate spheroid, with the axis of revolution coinciding with the  $\mathbf{e}_2$  direction in the particle-fixed frame, these expressions are given in the form

$$K_{11} = K_{33} = 16\pi a \frac{\beta^2 - 1}{\frac{2\beta^2 - 3}{\sqrt{\beta^2 - 1}} \ln(\beta + \sqrt{\beta^2 - 1}) + \beta}, \quad (\text{A7})$$

$$K_{22} = 8\pi a \frac{\beta^2 - 1}{\frac{2\beta^2 - 1}{\sqrt{\beta^2 - 1}} \ln(\beta + \sqrt{\beta^2 - 1}) - \beta}, \quad (\text{A8})$$

$$\Omega_{11} = \Omega_{33} = \frac{16\pi}{3} \frac{a^3(\beta^4 - 1)}{\frac{2\beta^2 - 1}{\sqrt{\beta^2 - 1}} \ln(\beta + \sqrt{\beta^2 - 1}) - \beta}, \quad (\text{A9})$$

$$\Omega_{22} = \frac{16\pi}{3} \frac{a^3(\beta^2 - 1)}{\frac{-1}{\sqrt{\beta^2 - 1}} \ln(\beta + \sqrt{\beta^2 - 1}) + \beta}, \quad (\text{A10})$$

$$Q_{11} = Q_{33} = \frac{16\pi}{3} \frac{a(\beta^2 - 1)}{\frac{2\beta^2 - 1}{\sqrt{\beta^2 - 1}} \ln(\beta + \sqrt{\beta^2 - 1}) - \beta}, \quad (\text{A11})$$

$$Q_{22} = \frac{8\pi}{3} \frac{a(\beta^2 - 1)}{\frac{-1}{\sqrt{\beta^2 - 1}} \ln(\beta + \sqrt{\beta^2 - 1}) + \beta}, \quad (\text{A12})$$